IEEE Access
Multidisciplinary | Rapid Review | Open Access Journal

Received February 13, 2019, accepted March 4, 2019, date of publication March 12, 2019, date of current version April 1, 2019.

Digital Object Identifier 10.1109/ACCESS.2019.2904307

Design of Compact Tri-Band Gysel Power Divider With Zero-Degree Composite Right-/Left-Hand Transmission Lines

FU-XING LIU, YANG WANG, SHI-PENG ZHANG, AND JONG-CHUL LEE, (Senior Member, IEEE)
Department of Radio Science and Engineering, Kwangwoon University, Seoul 139-701, South Korea
Corresponding author: Jong-Chul Lee (jclee@kw.ac.kr)

This work was supported by the National Research Foundation of Korea under Grant NRF-2016R1D1A1B03935640.

ABSTRACT In this paper, a tri-band Gysel power divider (PD) based on zero-degree composite right-/left-handed (CRLH) transmission lines (TLs) is presented. Compared to the generalized design methods in which multiple passbands are realized by replacing conventional impedance transformers with quarter-wavelength CRLH-TLs, the employed zero-degree CRLH-TLs include high design flexibility for the characteristic impedance and phase responses of the composed left-handed and right-handed TLs, which can be used to separately control the bandwidths of the three passbands. In addition, the microstrip-to-slotline transition is utilized to replace the conventional 180° TL, which can expand the realizable range of the three center frequencies and reduce the circuit size, as well. The proposed theory is validated using two designs: One involves a broadband PD with a center frequency of 2.5 GHz, while the other is a tri-band PD centered at 3.5 GHz, 2.5 GHz, and 1.5 GHz. Good agreement between the simulated and measured results are obtained; for the first PD, a fractional 3-dB bandwidth of up to 116% is achieved, whereas, for the tri-band PD, a size reduction of 80% is achieved with good impedance matching and isolation performance.

INDEX TERMS Compact, Gysel power divider, high design flexibility, microstrip-to-slotline transition, triple passbands, zero-degree composite right-/ left-handed (CRLH) transmission line (TL).

I. INTRODUCTION

With the rapid development of wireless communication and other commercial applications of microwave/millimeter wave frequencies, research on conventional devices with enhanced performances becomes increasingly inevitable. As indispensable components in RF/ microwave circuits, power dividers (PDs) are extensively used in antenna arrays, modulators, power amplifiers, etc. Therefore, many previous PD studies focused on the bandpass properties [1], [2], ultra-wideband (UWB) applications [3], [4], size reduction [5], [6], broadband performance [7], [8], improved isolation [9], [10], and arbitrary dividing ratios [11], [12] have been presented.

Of late, due to the explosive development of multi-standard microwave systems, research on multi-band PDs is gaining significance. In order to meet these requirements, various dual-band [13]–[20], and tri-band PDs [21]–[26] have been proposed. In [21], a multi-section structure is utilized to realize a tri-band Wilkinson PD; however, it suffers from bad out-of-band rejection in the first two passbands. In [22], triple passbands are obtained through short-circuited stepped impedance and half-wavelength resonators; nevertheless, the use of a coupling structure leads to high loss (>4.2 dB) in all the bands. Meanwhile, designs using an open-/short-circuited stub to extend the input/output ports or phase shifters have been reported [23]–[26]; however, the PDs in [23] and [24] suffer from narrow bandwidth, while the performance of the PDs in [25]–[27] are limited by the passband of the conventional Wilkinson and Gysel PDs. In addition, coupled lines [28], [29], and additional lumped elements [18] can also be utilized for realizing multi-band PDs.

All the aforementioned multi-band PDs are realized using conventional microstrip lines, which have a fixed three times harmonic response and bulky size. Different from the conventional transmission lines (TLs), composite right-/ left-handed (CRLH) TLs can achieve quarter-wavelength at two arbitrary

The associate editor coordinating the review of this manuscript and approving it for publication was Xiu Yin Zhang.

frequencies due to the nonlinear positive phase response of the LH-TL (phase lead) and linear negative phase response of the RH-TL (phase lag); this characteristic has generated considerable interest in the design of multi-band PDs [30]–[33]. However, the CRLH-TL function in previous multiband schemes is limited to quarter-wavelength impedance transformers, in which configuration, the characteristic impedance and phase response of the composed RH-/ LH-TL are precisely required. Meanwhile, as the available values of the lumped elements in the market are limited, the realizable frequency ratios are not continuous. Although this shortcoming can be solved by using capacitors in series, inductors in parallel [31], or interdigital capacitors and stubs [32], [33], these methods will lead to considerable parasitic effects and higher fabrication difficulty due to the narrow gap in the interdigital structure.

In this paper, a new tri-band equal-split Gysel PD structure is proposed. Compared to previous research [27], the existing shortcomings, such as the bulky size and poor isolation performance, are addressed by redesigning the structure and rearranging the location of the multiband biasing network. A new 180° phase shifter based on microstrip-to-slotline transitions is utilized, which reduces the bulk and increases the range of the realizable center frequencies. In addition, the proposed structure features a high-power handling capability, and high design flexibility, wherein most of the parameters in the tri-band networks can be freely selected; this characteristic can also be utilized to control the bandwidths of the three passbands separately.

This paper is organized as follows: In section II, the proposed tri-band biasing network, microstrip-to-slotline type phase shifter and tri-band Gysel PD are introduced. The proposed design method is verified using a broadband PD working at 2.5 GHz, and a tri-band PD working at 3.5 GHz, 2.5 GHz, and 1.5 GHz, in section III. Finally, the paper is concluded in section IV.

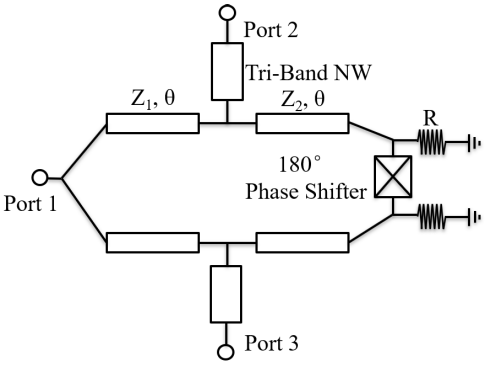

FIGURE 1. Structure of the proposed tri-band equal-split Gysel PD.

II. DESIGN THEORY

Fig. 1 displays the structure of the proposed tri-band equal-split Gysel PD, which is composed of RH-TL (Z_1 and Z_2) couples with the same quarter-wavelength, θ, a zero-degree CRLH-TL-based tri-band biasing network, two lumped isolation resistors, R, and a microstrip-to-slotline type 180° phase shifter. In the following subsections, the structure of the proposed tri-band biasing network is analyzed, and the design of the broadband and tri-band PDs is described.

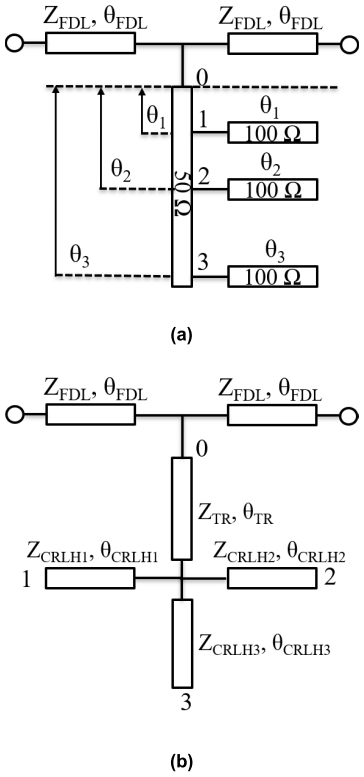

FIGURE 2. (a) Conventional and (b) proposed tri-band biasing network structures.

A. PROPOSED TRI-BAND BIASING NETWORK

The conventional tri-band biasing network, shown in Fig. 2(a), contains two impedance matching lines, Z_{FDL}, a 50-ohm trunk line, and three 100-ohm open-circuited stubs distributed at three specific positions, *1–3*. The design parameters for the biasing network are such that all the phase responses (θ_1, θ_2, and θ_3) are the same as that of 90° at the corresponding center frequencies (f_1, f_2, and f_3), respectively. Then, according to (1), positions *1–3*are first shorted by the corresponding quarter-wavelength open-circuited stub, and furtherly be transferred to open at point, *0*, as per (2).

$$Z_{IN} = -jZ_0 \cot\theta \tag{1}$$

$$Z_{IN} = jZ_0 \tan\theta \tag{2}$$

Hence, the conventional tri-band biasing network can be regarded as a combination of three 180° open-circuited stubs. However, this structure is bulky with a narrow bandwidth due to the high frequency dependence of the RH-TL phase response. From (1), the impedance of the open-circuit stub is related to $cot\theta$, which is an odd function with a 180° cycle.

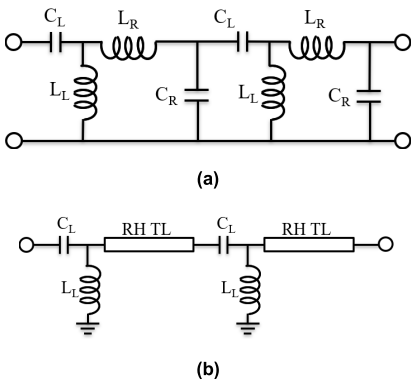

FIGURE 3. (a) Conventional and (b) utilized two-cell CRLH-TL structures.

Therefore, it is theoretically possible to replace the original 180° TLs, using three 0° TLs, respectively.

Fig. 2(b) depicts the structure of the proposed tri-band biasing network, which is composed of two impedance matching lines, Z_{FDL}, a common line, Z_{TR} for size reduction, and three sub-CRLH-TLs (Z_{CRLH1}, Z_{CRLH2}, and Z_{CRLH3}). All the phase responses from port-*0* to the end of the sub-CRLH stub at the corresponding frequencies are the same as that at 0°. Different from the previous CRLH-TL-based PD studies [30]–[33], in this structure, only the zero-degree phase response is precisely required, as shown in (3), where $\theta_{TR}(f_n)$ and θ_{CRLHn} represent the corresponding phase responses of the common line, Z_{TR}, and the sub-CRLH stub at the three center frequencies, respectively.

$$\theta_{TR}(f_n) + \theta_{CRLHn} = 0^\circ \tag{3}$$

Fig. 3 (a) illustrates the structure of the conventional two-celled CRLH-TL, in which all the RH- and LH-TLs are based on lumped elements; (4-7) are the design equations, where θ_R (θ_L), L_R (L_L), C_R (C_L), and Z_R (Z_L) represent the phase response, values of the lumped inductor and capacitor, and the impedance of the RH- (LH-) TL unit cell, respectively. Under this configuration, the size is compact; however, the use of several lumped elements can not only lead to complex mathematical calculations, but also introduce many parasitic effects. Moreover, because of the limited available values of the lumped elements in the market, it is difficult to achieve a precise zero-degree in practical applications. Therefore, the microtip-type RH-TL is utilized to overcome these shortcomings, as shown in Fig. 3(b); this structure can overcome the limitation of the lumped-element dispersive values by changing the length of the RH-TL to achieve a 0° phase response.

$$\theta_R = -\arctan\left[\frac{\omega\left(L_R/Z_R + C_R Z_R\right)}{2 - \omega^2 L_R C_R}\right] < 0^\circ \tag{4}$$

$$\theta_L = -\arctan\left[\frac{\omega\left(L_L/Z_L + C_L Z_L\right)}{1 - 2\omega^2 L_L C_L}\right] > 0^\circ \tag{5}$$

$$Z_R = \sqrt{L_R/C_R} \tag{6}$$

$$Z_L = \sqrt{L_L/C_L} \tag{7}$$

In the proposed tri-band biasing network, Z_{FDL} is another important parameter for impedance matching, when combined with another network. After applying the *ABCD* matrix to the structure, the following equation can be obtained:

$$\begin{bmatrix} \cos\theta_{FDL} & jZ_{FDL}\sin\theta_{FDL} \\ j\sin\theta_{FDL}/Z_{FDL} & \cos\theta_{FDL} \end{bmatrix} \begin{bmatrix} 1 & 0 \\ -jY_{BL} & 1 \end{bmatrix} \begin{bmatrix} \cos\theta_{FDL} & jZ_{FDL}\sin\theta_{FDL} \\ j\sin\theta_{FDL}/Z_{FDL} & \cos\theta_{FDL} \end{bmatrix} = \begin{bmatrix} \cos\theta_{BN} & jZ_{BN}\sin\theta_{BN} \\ j\sin\theta_{BN}/Z_{BN} & \cos\theta_{BN} \end{bmatrix} \tag{8}$$

where, Y_{BL} is the admittance seen from port *0* to the end of each sub-CRLH stub, and θ_{BN} and Z_{BN} are the phase response and equivalent impedance of the tri-band biasing network, respectively. According to the above analysis, $Y_{BL} = \infty$ at the three center frequencies; after, algebraic calculations, (8) can be expanded as

$$\theta_{BN} = 2\theta_{FDL}. \tag{9}$$

$$Z_{BN} = Z_{FDL}. \tag{10}$$

For the other parameters in the design of the tri-band biasing network, such as the impedance, Z_{TR}, cell numbers, *n,* and the phase of LH-TL, θ_{LH} can be freely selected, considering the bandwidth. For clear comparison, only one passband for six different cases was simulated using the AWR simulator. The utilized one-cell ($n = 1$) circuited model is given in Fig. 4(b). Besides the conventional RH-TL-based case-1, the design parameters for the other cases are listed in Table 1. Fig. 4 shows the return loss (S_{11}) for the six different cases centered at 2 GHz. Observing the six results, the following conclusions can be obtained: *1)* The proposed structure has a wider bandwidth than the conventional one, which characteristic is due to the fact that the utilized zero-degree CRLH-TL exhibits a mild frequency dependence of the phase response as shown in Fig. 5, in which two lines with 0° and -180° phase responses at 2 GHz are given. *2)* the bandwidth of the proposed biasing network can be improved by increasing the cell number, *n,* and the impedance of the common line (Z_{TR}) and sub-CRLH-TL ($Z_{sub-CRLH}$), or reducing the phase response of the LH-TL (θ_{LH}). It is to be noted that this characteristic can also be utilized to control the bandwidth of the three passbands in the tri-band design.

TABLE 1. Design parameters for the other five cases.

	Cell Number, n	θ_{LH}	Z_{TR}	$Z_{sub\text{-}CRLH}$
Case 1	———	———	50	100
Case 2	1	60	50	100
Case 3	1	60	50	30
Case 4	1	60	100	100
Case 5	1	30	50	100
Case 6	2	60	50	100

Finally, the design procedure of the proposed tri-band biasing network can be summarized as the calculation of

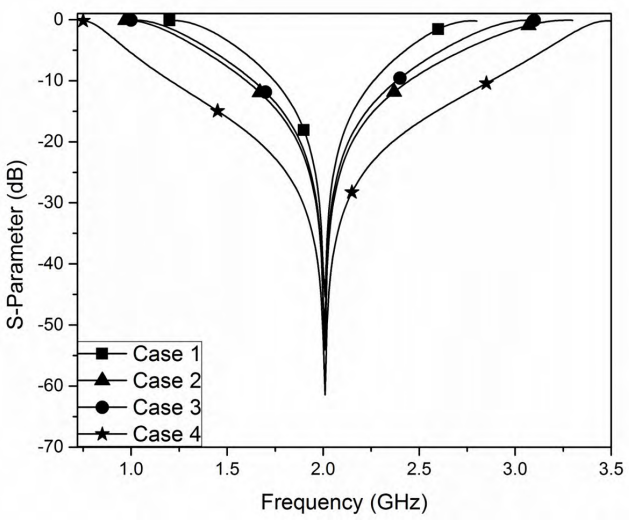

(a)

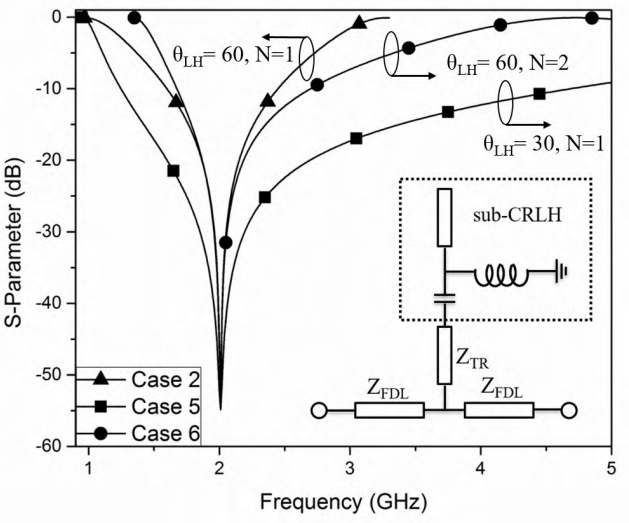

(b)

FIGURE 4. Simulated return loss (S_{11}) for six different cases.

the required values of the lumped inductors and capacitors in the LH-TL and the electrical length of the RH-TL using (5) and (7) to satisfy (3) at the corresponding frequencies, f_1, f_2, and f_3. For example, using (5), (7), (3) and f_1, the required parameters in branch 1 can be obtained. According to the above analysis, the phase response and impedance of the LH-cell can be selected freely, based on the available values of the lumped elements. It is to be noted that the length of the common line, Z_{TR}, should be lesser than the phase response of the LH-TL at the corresponding response, meanwhile, a long common line Z_{TR} can make the respective RH-TL short in the sub-CRLH part, resulting in a relatively small size. Further, the line Z_{FDL} is designed based on the impedance matching condition of the embedded network. When comes to the proposed tri-band PD, Z_{FDL} should be equal to the port impedance, Z_0, whereas the electrical length,

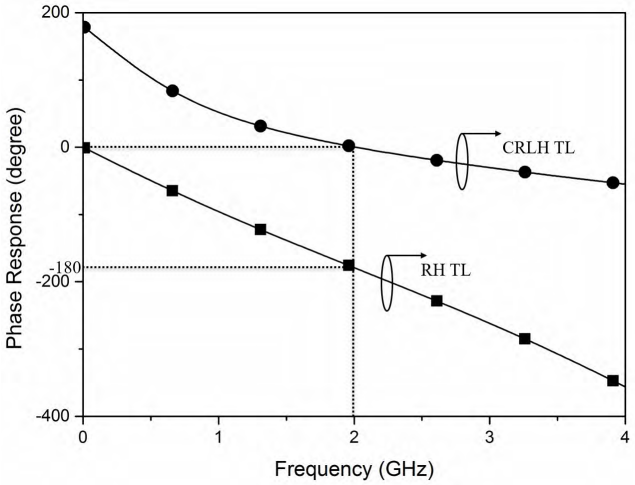

FIGURE 5. CRLH-TL and RH-TL phase response.

θ_{FDL}, can be freely selected. This characteristic is completely different from the design of the previous research [27], where both the characteristic impedance and the phase response of the TL play an important role in the impedance matching of the entire network.

B. PROPOSED TRI-BAND GYSEL POWER DIVIDER

The structure of the proposed tri-band PD as shown in Fig. 1, can be regarded as an integration of a tri-band biasing network and a broadband Gysel PD. Different from the previous research [27], the tri-band biasing network in this work is utilized to extend the output ports, which can result in good out-of-band rejection performance due to the fact that for the proposed configuration all the signals flow through the output ports can be processed by the proposed biasing network, while for the PD in [27], the biasing network also plays an important role in the whole network matching. However, for that structure, even under the unmatched condition, there still have some powers can be directly delivered to the output ports. According to the analysis in the previous sub-section, when the line Z_{FDL} is equal to the port impedance, Z_0, it will have no influence on the impedance matching of the broadband structure, which has already been analyzed [19], [34]. The design equations are

$$Z_1 = Z_2 = \sqrt{2}Z_0. \tag{11}$$

$$R = 2Z_0. \tag{12}$$

In the proposed broadband structure, the conventional narrow-band wavelength RH-TL is replaced with a new 180° phase shifter, similar to the design theory of hybrid couplers [35]–[40]. In this work, a microstrip-to-slotline type 180° phase shifter is employed, as shown in Fig. 6(a), which consists of two microstrip lines, two vertical metallic via, and an open-circuited slotline with one circular end. Note that in this phase shifter, the slotline can provide an open-circuit over a wide frequency band; if there is a continued ground, both ends of the slotline should connect with

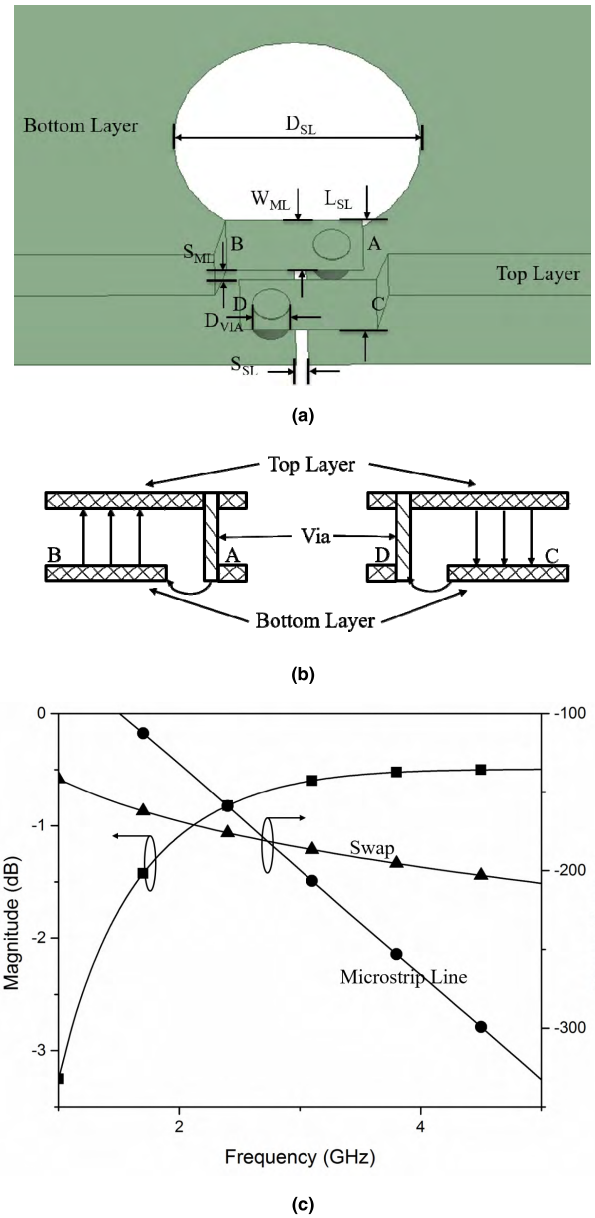

FIGURE 6. (a) Structure of the proposed 180° phase shifter, (b) Electric-field variation between the microstrip-to-slotline transitions *AB* and *CD*, and (c) Simulated insertion loss (S_{21}) and phase response of the proposed phase shifter.

additional circular stubs. Fig. 6(b) depicts the electric field variation between the two microstrip-to-slotline transitions *AB* and *CD*, in which the orientation of the electric field is first transferred from vertical to horizontal, and then transferred back to vertical, resulting in a 180° phase shift without additional delay lines. The detailed design procedure for the microstrip-to-slot line structure can be studied through the guidelines in [41]. In this work, the phase shifter is simulated, based on a Teflon substrate with a relative dielectric constant, $\varepsilon_r = 2.54$, thickness, $h = 0.54$ mm, and conductor height, $T = 0.018$ mm. The parameters in Fig. 6(a) include the diameter of the circular end: $D_{SL} = 4$ mm, width of the slot line: $S_{SL} = 0.2$ mm, length of the slot line: $L_{SL} = 2.5$ mm, diameter of the via hole: $D_{VIA} = 0.6$ mm, gap between *AB* and *CD*: $S_{ML} = 0.2$ mm, and width of the microstrip line: $W_{ML} = 1$ mm.

Fig. 6(c) shows the insertion loss (S_{21}) and phase response of the microstrip-to-slotline type phase shifter. In addition, a conventional microstrip line with the same 180° phase response at 2.7 GHz is also displayed for comparison. It is obvious that the utilized phase shifter has a milder curve than the conventional microstrip line. The $-170° - (-200)°$ phase response band can cover a frequency range of $2.1 - 4$ GHz, with an insertion loss lesser than 1 dB, resulting in a wider passband for the phase shifter-based Gysel PD.

In summary, the design procedure for the proposed tri-band Gysel PD can be summarized as follows:

1) Design the broadband PD using (11) and (12), where the lengths of Z_1 and Z_2 are the same as the quarter-wavelength at the center frequency, f_b.
2) Select the respective values of the lines and gaps in the phase shifter, based on the processing precision. A small S_{SL} and S_{MI} can minimize the radiation loss and the extra phase delay of the slot line. Therefore, $S_{SL} = S_{MI} = 0.2$ mm are set in this design. Then, select the diameter of the circular stub, $D_{SL,}$ and the length of the slotline, $L_{SL,}$ such that the range of the 180° phase shift can cover the center frequency, f_b.
3) Designate the three working frequencies f_1, f_2, and f_3, based on the passband of the broadband PD. Then, design the tri-band biasing network according to the above summarized design procedure. It is worth noting that in choosing the parameters of each branch, the corresponding bandwidth can also be taken into consideration. For example, if a wider bandwidth of the second passband is required, a larger cell number n, high Z_{CRLH2}, or less phase response of the LH-TL in the brunch 2 in Fig. 2(a) can be used.
4) Based on the initial parameters calculated above, use the EM simulator to optimize the values, and design considering the parasitic effects.

III. EXPERIMENT AND DISCUSSION

In this section, two Gysel PDs are designed, simulated, and fabricated to verify the proposed design method. One is a broadband PD operating at 2.5 GHz, that can be utilized to determine the realizable frequency range of the proposed tri-band PD. The other is a tri-band PD operating at 1.5 GHz, 2.5 GHz, and 3.5 GHz. All the following PDs are designed, based on a Teflon substrate with a relative dielectric constant, $\varepsilon_r = 2.54$, thickness, $h = 0.54$ mm, loss tangent, $\delta = 0.002$, and conductor height, $T = 0.018$ mm. The simulated and measured results are obtained using an *Ansoft* high frequency structure simulator (*HFSS*) and an *Agilent 8719ES* S-parameter vector network analyzer, respectively.

A. BROADBAND EQUAL-SPLIT POWER DIVIDER

In this broadband design, the phase shifter has the same parameters as the one proposed in section II B. The other

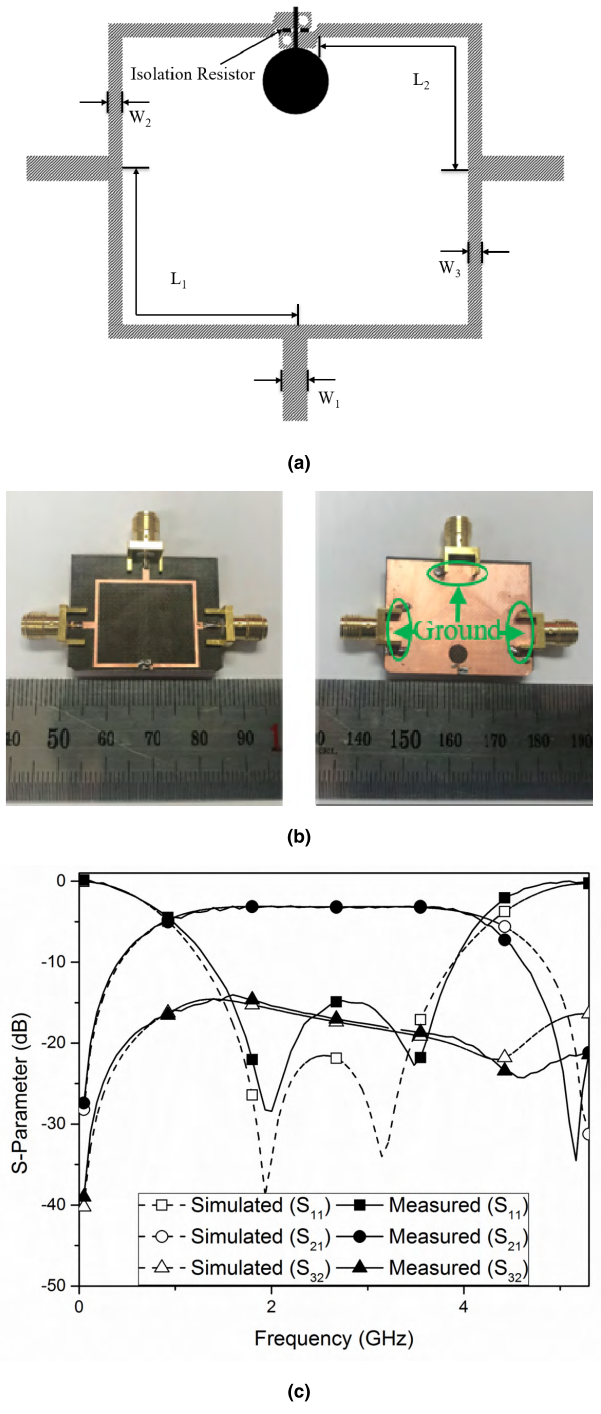

FIGURE 7. (a) Schematic, (b) photograph, and (c) simulated and measured results of the fabricated broadband Gysel PD.

parameters can be calculated using (11) and (12) with a port impedance $Z_0 = 50\ \Omega$, $Z_1 = Z_2 = 70.7\ \Omega$, and $R = 100\ \Omega$. Then, after transferring all the values to the line width and quarter-wave length at 2.5 GHz, the PD is designed as shown in Fig. 7(a), in which the two isolation resistors are 1005 chip resistors, the line widths $W_1 = 1.49$ mm, and $W_2 = W_3 = 0.83$ mm, and the line lengths $L_1 = 20.9$ mm, and $L_2 = 18$ mm.

Fig. 7(b) depicts the photograph of the fabricated broadband PD; the figure on the left is the top layer, and the one on the right is the bottom layer. Due to the elimination of the conventional wavelength TL, the size is reduced to $0.39\lambda_0 \times 0.30\lambda_0$, where λ_0 is the wavelength at 2.5 GHz. The simulated and measured results are shown in Fig. 7(c), in which the small difference between the EM and circuit model is mainly due to the limited fabrication accuracy, such as the slightly misalignment of the two layers, the inaccurate width of the slot line, and even since the length of the metal via is always longer than the height of the substrate, additional parasitic effects can also be introduced. By observing this figure, it is obvious that a broad 3-dB insertion loss (S_{21}) passband from 1.1–4 GHz can be obtained with good isolation of more than 14 dB in all the bands. In the passband, the measured maximum return loss (S_{11}) and isolation (S_{32}) are 28.4 dB and 20.1 dB, respectively, while the minimum insertion loss is 3.10 dB.

B. TRI-BAND EQUAL-SPLIT POWER DIVIDER

Based on the passband of the abovementioned PD, the three center frequencies $f_1 = 3.5$ GHz, $f_2 = 2.5$ GHz, and $f_3 = 1.5$ GHz are designated. The tri-band biasing network is then designed, according to the abovementioned design procedure, wherein the line impedance, Z_{FDL} should be Z_0 (50 Ω) for impedance matching; for the other parameters, only the relationship shown in (3) is strictly required. In this work, the impedance of the common line, Z_{TR}, and the sub-CRLH lines are freely selected as 50 Ω and 100 Ω, respectively. All the phase responses of the LH-TLs are set as 60° at the corresponding frequencies. The values of the lumped elements can be calculated using (5) and (7) as $I_1 = 4.7$ nH, $C_1 = 0.47$ pF, $I_2 = 6.7$ nH, $C_2 = 0.67$ pF, $I_3 = 11.2$ nH, and $C_3 = 1.12$ pF, where I_1 (I_2, I_3) and C_1 (C_2, C_3) are the values of the lumped inductor and capacitor calculated at f_1 (f_2, f_3), respectively. However, as mentioned previously, only limited values of the lumped elements are available; hence, finally, the values are selected as $I_1 = 1.5$ nH, $C_1 = 0.5$ pF, $I_2 = 4.7$ nH, $C_2 = 0.75$ pF, $I_3 = 12$ nH, and $C_3 = 1.2$ pF. Thereby, the phase responses of the relevant LH-TL at the three center frequencies are 77.1°, 68°, and 50°, respectively. Then, based on the phase response of the LH-TL, the phase response of the common line, θ_{TR}, is selected as $-60°$ at f_1. For the other frequencies, the phase responses, θ_{TR}, are $-43°$ and $-26°$, respectively. Then according to (3), the required electrical length of the RH-TL in the corresponding sub-CRLH are $-17.1°$, $-33.9°$, and $-24°$, respectively. After transferring all the calculated values to the line length and width, and optimizing the parameters, after considering the parasitic effects, the tri-band PD is finally designed as shown in Fig. 8(a). In this, $L_1 = 4.6$ mm, $L_2 = 0.2$ mm, $L_3 = 7.8$ mm, $L_4 = 1$ mm, $L_5 = 1.8$ mm, $W_1 = 1.2$ mm, $W_2 = 0.4$ mm, $W_3 = 0.6$ mm, $W_4 = 0.4$ mm, $W_5 = 0.4$ mm, $W_6 = 1.49$ mm, the diameter of the via $D_1 = 0.6$ mm, and all the utilized lumped inductors and capacitors are 2012 chip elements. It is to be noted that there is a relatively large difference

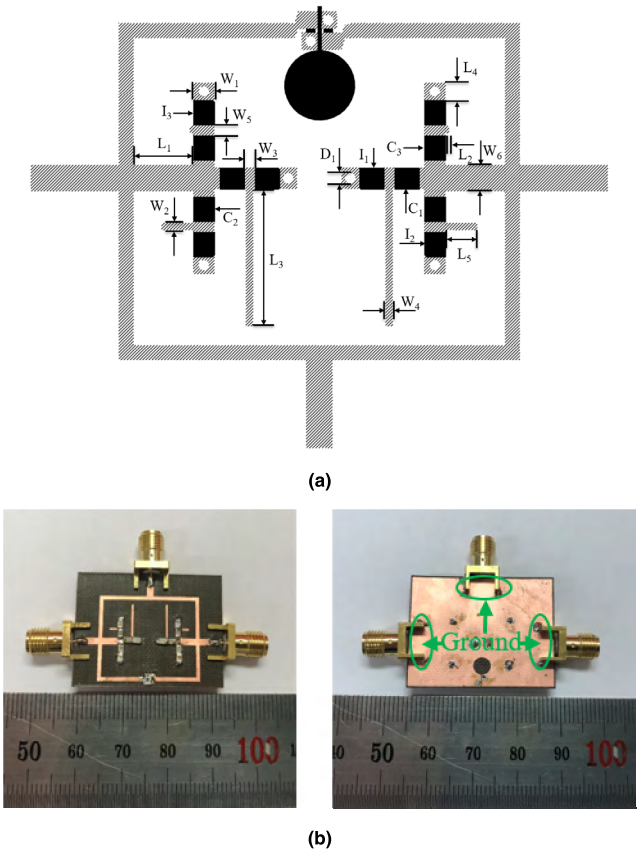

FIGURE 8. (a) Schematic and (b) photograph for the fabricated tri-band Gysel PD.

between the optimized parameters and the calculated ones at f_3, which is due to the LH-TL characteristic, wherein the phase response is more easily influenced by the values of the lumped elements at lower frequencies.

Fig. 8(b) depicts the photograph of the fabricated PD, the image on the left is the top layer, while the one on the right is the bottom layer. The measured maximum return loss (S_{11}) and minimum insertion loss (S_{21}) at the three passbands are 24.3 dB/16.5 dB/14.9 dB and 3.31 dB/3.15 dB/3.13 dB, respectively, as shown in Fig. 9(a). A good isolation can also be obtained that the minimum loss at the third passband is 14 dB while those for the other bands are 20 dB each. The relatively poor performance at the third passband is mainly due to the performance of the broadband PD, in which the isolation and return loss are 14.3 dB and 13.3 dB, respectively, as shown in Fig. 7(c). Good agreement between the simulated and measured results can be observed. In addition, the phase and amplitude imbalance are below 0.5 dB and 4°, respectively, in all the passbands. capability.

In addition, a comparison with previous tri-band PDs with respect to the PD type, utilized technology, composed isolation network, normalized size (where λ_0 is the average wavelength of the first and second center frequencies), capability of introducing additional passbands, out-of-band rejection, and high-power handling capability is listed in Table 2, which shows that the proposed PD is the first multi-band PD using

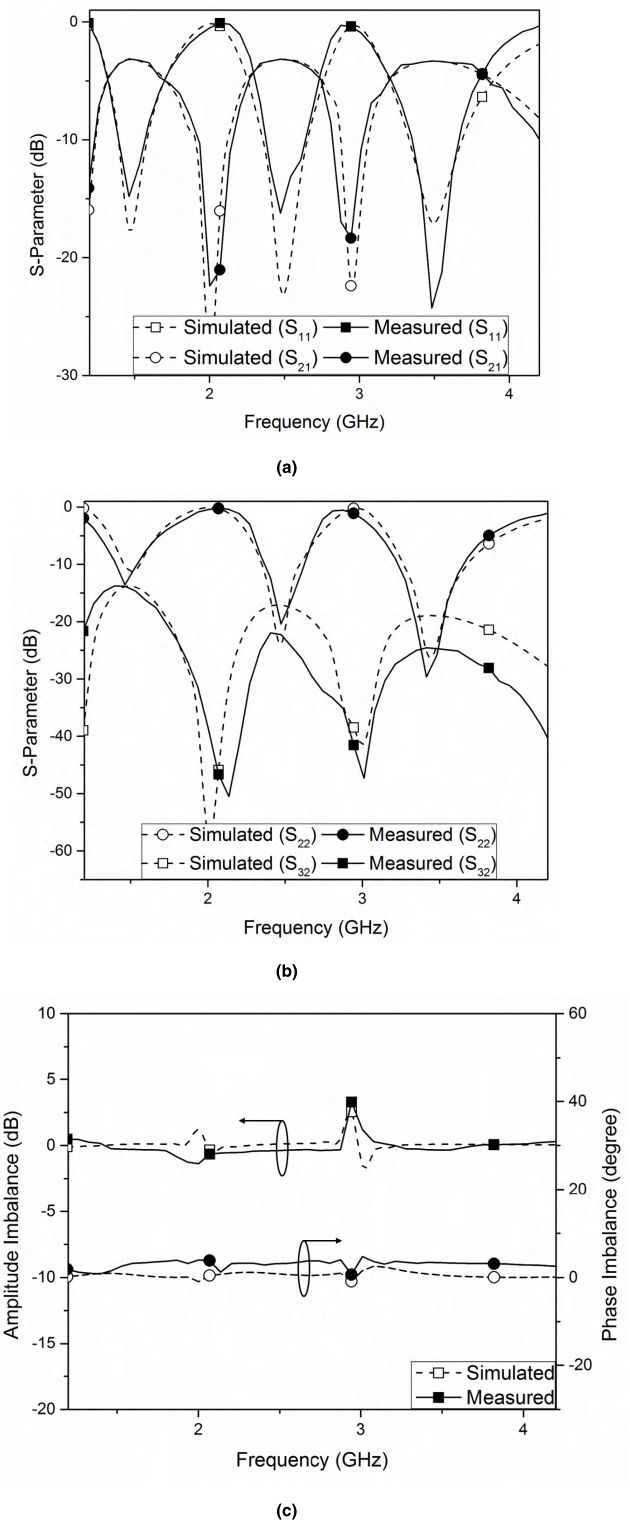

FIGURE 9. (a) Simulated and measured input port return loss (S_{11}) and insertion loss (S_{21}), (b) output port return loss (S_{22}) and isolation (S_{32}), and (c) phase and amplitude imbalance for the fabricated tri-band Gysel PD.

zero-degree TLs under smallest size, high design flexibility, high-power handling capability, and good out-of-band rejection, simultaneously. Moreover, it is worth noting that

TABLE 2. Comparison with previous designs.

Ref	*CF f_1/ f_2/ f_3 (GHz)*	*Type*	*Technology*	*Isolation Network*	*Size*	*Substrate ($\varepsilon_{r/h}$)*	*CAB*	*OTR*	*HPH*
[21]	0.90/ 1.17/ 2.43	Wilkinson	multi-section structure	3-resistors	$0.51 \times 0.29\ \lambda_0^2$	3.45/1.57	no	low	no
[22]	3.49/ 4.13/ 5.57	Wilkinson	Stepped impedance resonator	1-resistor	$0.60 \times 0.55\ \lambda_0^2$	3.5/ 0.5	no	high	no
[23]	1.01/ 2.40/ 2.07	Gysel	Additional short- and open-end stubs	2-resistors	$0.60 \times 0.70\ \lambda_0^2$	2.2/ 0.5	no	low	yes
[24]	1.02/ 2.57/ 3.06	Wilkinson	Additional short- and open-end stubs	1-resistor	$0.50 \times 0.37\ \lambda_0^2$	2.55/ 0.8	no	low	no
[25]	1.50/ 1.90/ 2.35	Wilkinson	180° open-end stub-based network	1-resistor	$0.61 \times 0.47\ \lambda_0^2$	3.48/ 0.78	yes	high	no
[26]	3.06/ 2.52/ 2.00	Gysel	180° open-end stub-based network	2-resistors	$0.61 \times 0.49\ \lambda_0^2$	2.45/ 0.54	yes	medium	yes
[27]	3.07/ 2.47/ 1.93	Gysel	180° open-end stub-based network	2-resistors	$0.88 \times 0.83\ \lambda_0^2$	2.45/ 0.54	yes	medium	yes
[28]	1.57/ 2.45/ 3.50	Wilkinson	Additional short- and open-end stubs	2-resistors	$0.61 \times 0.47\ \lambda_0^2$	2.65/ 1	no	high	no
[29]	1.00/ 1.30/ 3.30	Wilkinson	Coupled line	1-resistor	$1.45 \times 1.45\ \lambda_0^2$	4.33/ 1.6	no	medium	no
[30]	0.84/ 1.28/1.68	Wilkinson	CRLH-TL & multi-section structure	1-resistor	$0.99 \times 0.24\ \lambda_0^2$	10.2/ 1.27	no	low	no
This Work	1.46/ 2.47/ 3.48	Gysel	0° open-end stub-based network	2-resistors	$0.39 \times 0.30\ \lambda_0^2$	2.45/ 0.54	yes	high	yes

Ref: Reference; CAB: Capability of Employing Additional Passbands; OTR: Out-of- Band Rejection; HPH: High-Power Handling Capability

when the proposed PD needs to be used under a high-power, the chip resistor should be replaced by a 50-ohm high-power resistor or a high-power isolation network with 50-ohm equivalent impedance, and additional aluminum block should be made for good heat dissipation.

IV. CONCLUSION

In this paper, a new design method of a tri-band Gysel PD was presented and verified using two fabricated PDs. Compared to the previous CRLH-TL-based multiband PDs, a new type of multi-band biasing network composed of zero-degree TLs is utilized, which results in a high design freedom and good out-of-band rejection performance. Additional passbands can be easily introduced by employing additional sub-CRLH-TLs. According to Table 2, the size of the fabricated PD is compact, which can also be further reduced by employing slow-wave TLs or proper bending of the microstrip lines. Moreover, due to the two grounded resistors, the proposed PD also features high-power handling capability, making it more suitable for real applications.

REFERENCES

[1] F.-X. Liu, W. Yang, X.-Y. Zhang, and J.-C. Lee, "A power divider with high-power handling capability and enhanced selectivity performance," *Microw. Opt. Technol. Lett.*, vol. 60, no. 8, pp. 1993–1997, Jun. 2018.

[2] F.-X. Liu, W. Yang, and J.-C. Lee, "A coupled line type of Wilkinson power divider with flexible bandwidth and out-of-band rejection performance," *Microw. Opt. Technol. Lett.*, vol. 60, no. 7, pp. 1778–1782, Jul. 2018.

[3] Y. Guo and R. Xu, "Ultra-wideband power splitting/combining technique using zero-degree left-handed transmission lines," *J. Electromagn. Waves Appl.*, vol. 21, no. 8, pp. 1109–1118, Apr. 2012.

[4] K. Song and Q. Xue, "Novel ultra-wideband (UWB) multilayer slotline power divider with bandpass response," *IEEE Microw. Compon. Lett.*, vol. 20, no. 1, pp. 13–15, Jan. 2010.

[5] K. Rawat and F. M. Ghannouchi, "A design methodology for miniaturized power dividers using periodically loaded slow wave structure with dual-band applications," *IEEE Trans. Microw. Theory Techn.*, vol. 57, no. 12, pp. 3380–3388, Dec. 2009.

[6] X. Ren, K. Song, F. Zhang, and B. Hu, "Miniaturized Gysel power divider based on composite right/left-handed transmission lines," *IEEE Microw. Wireless Compon. Lett.*, vol. 25, no. 1, pp. 22–24, Jan. 2015.

[7] C.-H. Tseng and C.-L. Chang, "A broadband quadrature power splitter using metamaterial transmission line," *IEEE Microw. Wireless Compon. Lett.*, vol. 18, no. 1, pp. 25–27, Jan. 2008.

[8] M. A. Antoniades and G. V. Eleftheriades, "A broadband series power divider using zero-degree metamaterial phase-shifting lines," *IEEE Microw. Wireless Compon. Lett.*, vol. 15, no. 11, pp. 808–810, Nov. 2005.

[9] J. Guan, L. Zhang, Z. Sun, Y. Leng, and Y. Peng, "Designing power divider by combining Wilkinson and gysel structure," *Electron. Lett.*, vol. 48, no. 13, pp. 769–770, Jun. 2012.

[10] J.-C. Kao, Z.-M. Tsai, K.-Y. Lin, and H. Wang, "A modified Wilkinson power divider with isolation bandwidth improvement," *IEEE Trans. Microw. Theory Techn.*, vol. 60, no. 9, pp. 2768–2780, Sep. 2012.

[11] Y. Wu, Y. Liu, and S. Li, "A modified Gysel power divider of arbitrary power ratio and real terminated impedances," *IEEE Microw. Wireless Compon. Lett.*, vol. 21, no. 11, pp. 601–603, Nov. 2011.

[12] K.-X. Wang, X. Y. Zhang, and B.-J. Hu, "Gysel power divider with arbitrary power ratios and filtering responses using coupling structure," *IEEE Trans. Microw. Theory Techn.*, vol. 62, no. 3, pp. 431–440, Mar. 2014.

[13] K.-K. M. Cheng and C. Law, "A novel approach to the design and implementation of dual-band power divider," *IEEE Trans. Microw. Theory Techn.*, vol. 56, no. 2, pp. 487–492, Feb. 2008.

[14] Y. C. Li, Q. Xue, and X. Y. Zhang, "Single- and dual-band power dividers integrated with bandpass filters," *IEEE Trans. Microw. Theory Techn.*, vol. 61, no. 1, pp. 69–76, Jan. 2013.

[15] Y. Wu, Y. Liu, Y. Zhang, J. Gao, and H. Zhou, "A dual band unequal Wilkinson power divider without reactive components," *IEEE Trans. Microw. Theory Techn.*, vol. 57, no. 1, pp. 216–222, Jan. 2009.

[16] M. J. Park, "Two-section cascaded coupled line Wilkinson power divider for dual-band applications," *IEEE Microw. Wireless Compon. Lett.*, vol. 19, no. 4, pp. 188–190, Apr. 2009.

[17] Y. Wu, Y. Liu, and Q. Xue, "An analytical approach for a novel coupled-line dual-band Wilkinson power divider," *IEEE Trans. Microw. Theory Techn.*, vol. 59, no. 2, pp. 286–294, Feb. 2011.

[18] X. Wang, I. Sakagami, K. Takahashi, and S. Okamura, "A generalized dual-band Wilkinson power divider with parallel L, C, and R components," *IEEE Trans. Microw. Theory Techn.*, vol. 60, no. 4, pp. 952–964, Apr. 2012.

[19] F. Lin, Q.-X. Chu, Z. Gong, and Z. Lin, "Compact broadband Gysel power divider with arbitrary power-dividing ratio using microstrip/slotline phase inverter," *IEEE Trans. Microw. Theory Techn.*, vol. 60, no. 5, pp. 1226–1234, May 2012.

[20] Z. Sun, L. Zhang, Y. Yan, and H. Yang, "Design of unequal dual-band Gysel power divider with arbitrary termination resistance," *IEEE Trans. Microw. Theory Techn.*, vol. 59, no. 8, pp. 1955–1962, Aug. 2011.
[21] M. Chongcheawchamnan, S. Patisang, M. Krairiksh, and I. D. Robertson, "Tri-band Wilkinson power divider using a three-section transmission-line transformer," *IEEE Microw. Wireless Compon. Lett.*, vol. 16, no. 8, pp. 452–454, Aug. 2006.
[22] K. Song, M. Fan, F. Zhang, Y. Zhu, and Y. Fan, "Compact triple-band power divider integrated bandpass-filtering response using short-circuited SIRs," *IEEE Trans. Compon., Packag., Manuf. Technol.*, vol. 7, no. 7, pp. 1144–1150, Jul. 2017.
[23] M. Hayati, S.-A. Malakooti, and A. Abdipour, "A novel design of triple-band Gysel power divider," *IEEE Trans. Microw. Theory Techn.*, vol. 61, no. 10, pp. 3558–3567, Oct. 2013.
[24] Q.-X. Chu, F. Lin, Z. Lin, and Z. Gong, "Novel design method of tri-band power divider," *IEEE Trans. Microw. Theory Techn.*, vol. 59, no. 9, pp. 2221–2226, Sep. 2011.
[25] B. M. Abdelrahman, H. N. Ahmed, and A. I. Nashed, "A novel tri-band Wilkinson power divider for multiband wireless applications," *IEEE Microw. Wireless Compon. Lett.*, vol. 27, no. 10, pp. 891–893, Oct. 2017.
[26] F.-X. Liu, Y. Wang, X.-Y. Zhang, C.-H. Quan, and J.-C. Lee, "A size-reduced tri-band Gysel power divider with ultra-wideband harmonics suppression performance," *IEEE Access*, vol. 6, pp. 34198–34205, 2018.
[27] F.-X. Liu, Y. Wang, X.-Y. Zhang, C.-H. Quan, and J.-C. Lee, "A new multi-band Gysel power divider," in *IEEE MTT-S Int. Microw. Symp. Dig.*, Chengdu, China, May 2018, pp. 1–4.
[28] W. Q. Liu, F. Wei, and X. W. Shi, "A compact tri-band power divider based on triple-mode resonator," *Prog. Electromagn. Res.*, vol. 138, pp. 283–291, Jun. 2013.
[29] H.-H. Chen and Y.-H. Pang, "A tri-band Wilkinson power divider utilizing coupled lines," in *Proc. APSURSI*, Spokane, WA, USA, Jul. 2011, pp. 25–28.
[30] I.-H. Lin, M. DeVincentis, C. Caloz, and T. Itoh, "Arbitrary dual-band components using composite right/left-handed transmission lines," *IEEE Trans. Microw. Theory Techn.*, vol. 52, no. 4, pp. 1142–1149, Apr. 2004.
[31] A. Genc and R. Baktur, "Dual- and triple-band Wilkinson power dividers based on composite right- and left-handed transmission lines," *IEEE Trans. Compon. Packag. Manuf. Technol.*, vol. 1, no. 3, pp. 327–334, Mar. 2011.
[32] H. L. Zhang, B. J. Hu, and X. Y. Zhang, "Compact equal and unequal dual-frequency power dividers based on composite right-/left-handed transmission lines," *IEEE Trans. Ind. Electron.*, vol. 59, no. 9, pp. 3464–3472, Sep. 2012.
[33] X. Ren, K. Song, M. Fan, Y. Zhu, and B. Hu, "Compact dual-band Gysel power divider based on composite right- and left-handed transmission lines," *IEEE Microw. Wireless Compon. Lett.*, vol. 25, no. 2, pp. 82–84, Feb. 2015.
[34] L. Chiu and Q. Xue, "A parallel-strip ring power divider with high isolation and arbitrary power-dividing ratio," *IEEE Trans. Microw. Theory Techn.*, vol. 55, no. 11, pp. 2419–2426, Nov. 2007.
[35] C.-W. Kao and C. H. Chen, "Novel uniplanar 180° hybrid-ring couplers with spiral-type phase inverters," *IEEE Microw. Guided Wave Lett.*, vol. 10, no. 10, pp. 412–414, Oct. 2000.
[36] T. Wang and K. Wu, "Size-reduction and band-broadening design technique of uniplanar hybrid ring coupler using phase inverter for M(H)MIC's," *IEEE Trans. Microw. Theory Techn.*, vol. 47, no. 2, pp. 198–206, Feb. 1999.
[37] B. R. Heimer, L. Fan, and K. Chang, "Uniplanar hybrid couplers using asymmetrical coplanar striplines," *IEEE Trans. Microw. Theory Techn.*, vol. 45, no. 12, pp. 2234–2240, Dec. 1997.
[38] W. J. Feng, Q. Xue, and W. Che, "Compact planar magic-T based on the double-sided parallel-strip line and the slotline coupling," *IEEE Trans. Microw. Theory Techn.*, vol. 58, no. 11, pp. 2915–2923, Nov. 2010.
[39] K. U. Yen, E. J. Wollack, and J. Papapolymerou, "A broadband planar magic-T using microstrip-slotline transitions," *IEEE Trans. Microw. Theory Techn.*, vol. 56, no. 1, pp. 172–177, Jan. 2008.
[40] M. E. Bialkowski and Y. Wang, "Wideband microstrip 180° hybrid utilizing ground slots," *IEEE Microw. Wireless Compon. Lett.*, vol. 20, no. 9, pp. 495–497, Sep. 2010.
[41] B. Shuppert, "Microstrip/slotline transitions: Modeling and experimental investigation," *IEEE Trans. Microw. Theory Techn.*, vol. 36, no. 8, pp. 1272–1282, Aug. 1988.

FU-XING LIU received the B.S. degree in integrated circuit design and integration system from the Qingdao University of Science and Technology (QUST), China, in 2016. He is currently pursuing the Ph.D. degree, under the supervision of Prof. J.-C. Lee, with the WICS Laboratory, Kwangwoon University, South Korea.

His research interests include microwave passive devices, electromagnetic metamaterials, and RF sensors.

YANG WANG received the B.S. degree in electric and information engineering from the Harbin Institute of Technology (HIT), China, in 2013. He is currently pursuing the Ph.D. degree, under the supervision of Prof. J.-C. Lee, with the WICS Laboratory, Kwangwoon University, South Korea.

His research interests include RF design and electromagnetic metamaterials.

SHI-PENG ZHANG received the B.S. and M.S. degrees in wireless communication engineering from the College of Electronics and Information Engineering, Kwangwoon University, South Korea, in 2014 and 2016, respectively, where he is currently pursuing the Ph.D. degree, under the supervision of Prof. J.-H. Kim, with the SRS Laboratory.

His research interests include RF power amplifier design, RF device reliability, and millimeter wave radar systems.

JONG-CHUL LEE (M'92–SM'07) received the B.S. and M.S. degrees in electronic engineering from Hanyang University, Seoul, South Korea, in 1983 and 1985, respectively, the M.S. degree from Arizona State University, Tempe, AZ, USA, in 1989, and the Ph.D. degree from the Texas A&M University, College Station, TX, USA, in 1994, all in electrical engineering. From 1994 to 1996, he was a Senior Researcher with the Photonic Devices Laboratory, System IC Research and Development Laboratory, Hyundai Electronics Ind. Co., Ltd., South Korea, where he was involved in the development of several high speed laser diodes and photo diodes, and transmitter/receiver modules. Then, he joined the Department of Radio Science and Engineering, Kwangwoon University, Seoul, where he is currently a Professor. He has been a Guest Professor with the Department of Electronics and Communication, Harbin Institute of Technology, since 2001. He was a Visiting Scholar with the Department of Electrical and Computer Engineering, University of California San Diego, from 2002 to 2004. He also served as a Project Director at the ITRC RFIC Center, Kwangwoon University, which was funded by the Ministry of Information and Communication, from 2000 to 2007. He has authored and co-authored over 200 papers in international conferences and journals. He currently participates in several government projects related to the microwave and millimeter wave devices. His research interests include RF MEMS, RF application for ferroelectric materials, microwave and millimeter-wave passive and active devices, electromagnetic metamaterials, IT convergence with biomedical devices, and energy harvesting devices.